Proceedings of GT2006
ASME Turbo Expo 2006: Power for Land, Sea and Air
May 8-11, 2006, Barcelona, Spain

GT2006-91008

ANALYSIS OF LEAKAGE FLOW AND DYNAMIC CHARACTERISTICS IN FLOATING RING SEALS FOR HIGH PRESSURE TURBOPUMP

Yong-Bok Lee, Chang-Ho Kim
Korea Institute of Science and Technology, Tribology Research Center,
Seoul, 136-791, Republic of Korea
and
Wenbo Duan , Fulei Chu
Department of Precision Instruments and Mechanology, Tsinghua Univeristy
Beijing, 100084, People's Republic of China

ABSTRACT

Because the solutions based on the numerical integration of the complete Navier-Stokes equations can be very time-consuming, the bulk-flow model was used for calculating the static and the dynamic characteristics of floating ring seals. The bulk-flow model is governed by three partial differential equations on eccentric working conditions with steepest descent method to find the seal's equilibrium position efficiently. A finite difference scheme has been used to solve the nonlinear governing equations. Compared to Nelson and Nguyen's Fast Fourier Transform Method, this scheme has better consistency. Perturbation analysis of the flow variables yields a set of zeroth and first-order equations. The SIMPLE algorithm is used to integrate the system of bulk-flow equations. Comparisons of the numerical predictions (lock-up eccentricity ratio, leakage flow rate and rotordynamic coefficients) with Ha's results, which were formulated using the Fourier series, and experimental data are presented subsequently. [*Keywords:* Floating ring seals; Turbopump]

INTRODUCTION

In the turbopump of liquid rocket engine (LRE) system, the floating ring seal could be used to minimize the radial clearance without or minimal the rubbing phenomenon. Figure 1 presents the structural arrangement of the floating ring seal. The "floating ring" is inserted in between the rotor and the pump housing, and the axial motion of floating ring is restrained by a clamping nut. It is in contact with the rotor surface at the maximum eccentricity position when the pump is not operating. When the pump begins to operate, the pressure induced by the buck-flow liquid attaches the floating ring on the supporting ring surface. Simultaneously, the hydrodynamic force in the radial direction is generated like the case of fluid film bearing, and moves the floating ring to the geometric center of the rotor. After the hydrodynamic force and the friction force achieve an equilibrium condition, the floating ring is locked up at that eccentricity. Then, the floating ring seal begins to act like an

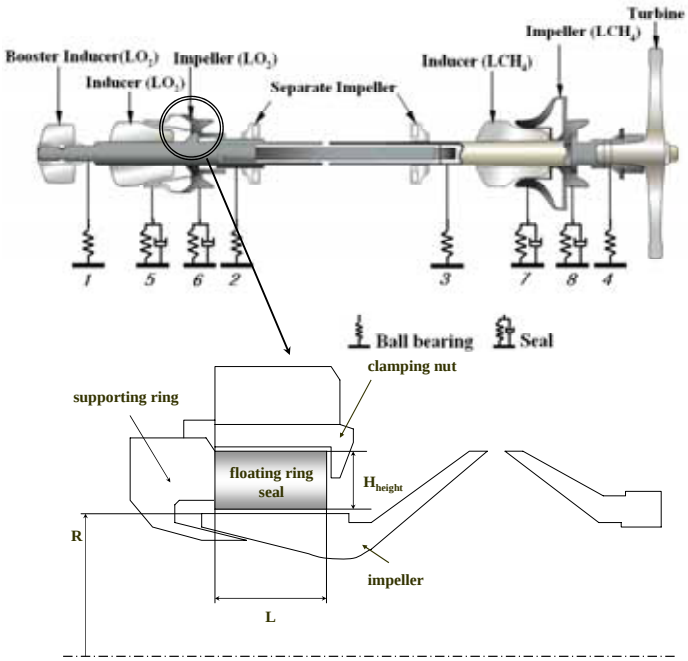

Figure 1. Structural arrangement of a floating ring seal.

annular plain seal. Theories for predicting the static and the dynamic characteristics of floating ring seals have been under development for the last three decades. Due to the enlarged clearances, combined with a high pressure drop across the seal, the reduced Reynolds number characterizing the annular seal flow is highly turbulent. Hence, the usual simplifications of the lubrication theory and the classical Reynolds equation are completely inappropriate for typical annular seal analyses. Bulk-flow versions of Navier-Stokes equations have been used in the present analysis.

Kirk [1-2] et al did an initial work for the analysis and testing of floating ring seals and the general Reynolds equations were introduced for the theoretical analysis of hydrodynamic oil film. Rotordynamic characteristics were obtained by using the finite difference method. Ha *et al.* [3] further explained the working process of the floating ring seal and their advantages compared to conventional non-contact type seals (such as plain, labyrinth, and damper seals). Floating ring seals could be used to minimize radial clearance and improve leakage performance. Nelson and Nguyen's Fast Fourier Transform Method was used to calculate the leakage flowrate and dynamic coefficients in the paper. This method considers the rotational symmetry of the seal and develops a numerical solution in terms of a fast Fouier transform in the circumferential direction. However Nelson and Nguyen's method lacks consistency, for it uses a simplification of the variables to transform the two-dimensional partial differential equations to one-dimensional axial differential equations. In this paper, it is presumed that the exact solution for small perturbation about the centered position is in fact a simple harmonic. Since a large number of angular function components are required in the floating ring seal's operating eccentricity and convergence is impaired. After the floating ring was locked up at a specific position, the floating ring seal began to act like an eccentric annular plain seal. The analysis method of the eccentric annular plain seal can be used to predict the static and dynamic characteristics of the floating ring seal. Childs et al. [4-6] have provided a fundamental program for the analysis and testing of concentric turbulent annular seals. San Andres [7] developed the turbulent flow analysis in an annular pressure seal of arbitrary nonuniform clearance. All major effects such as inlet preswirl effects, and local variations of friction factors by Moody's formulas were taken into account. A finite difference method was used to solve the nonlinear governing equations. The SIMPLE Consistent algorithm of Van Doormaal and Raithby [8] was used to accelerate convergence in the solution of the difference equations.

The analysis developed in this paper uses a steepest descent method to determine the floating ring seal's lock-up position efficiently. Bulk-flow model is introduced for the analysis of turbulent flow floating ring seals. Static and dynamic characteristics are predicted, based on the perturbation analysis and a finite difference scheme. The theoretical results are then compared to the results of Ha's analysis and Lee's experimental data taken from the literature [9].

NOMENCLATURE

a_1,b_2	constant coefficients in Moody's friction formulas
a_3	friction coefficient in Moody's friction formulas, b_3/R_e
b	dimensionless shaft rotating speed, $R\varpi/\bar{V}$
$\bar{C}$	nominal radial clearance [m]
C_{ij}	damping coefficients [Ns/m]
e_0	shaft eccentricity
e_s, e_r	absolute surface roughness at stator and rotor [m]
F_{dyn}	hydrodynamic force [N]
F_N	normal force [N]
F_μ	friction force [N]
$F_X^{(1)}$, $F_Y^{(1)}$	fluid perturbation forces in X and Y directions [N]
f_s, f_r	turbulent friction factors at stator and rotor surfaces

h	dimensionless film thickness, H/ $\bar{C}$
H_{height}	floating ring height [m]
h_x, h_y	cos(θ) and sin(θ)
K_{ij}	stiffness coefficients [MN/m]
L	floating ring seal length [m]
M_{ij}	inertia coefficients [kg]
P	dimensionless fluid pressure, P/ρ $\bar{V}^2$
P_s	sump pressure of floating ring seal [Pa]
P_r	reservoir pressure of floating ring seal [Pa]
R	rotor radius [m]
R_e	Reynolds number, 2 $\bar{C}\bar{V}$ ρ/μ
R_0	floating ring seal radius [m]
T	fluid transit time [s], $L/\bar{V}$
τ	dimensionless time, t/T
u_z	dimensionless axial velocity, $U_z/\bar{V}$
u_θ	dimensionless circumferential velocity, $U_\theta/R\varpi$
u_s	dimensionless bulk-flow velocity relative to the stator surface, $U_s/\bar{V}$
u_r	dimensionless bulk-flow velocity relative to the rotor surface, $U_r/\bar{V}$
$\bar{V}$	average axial velocity [m/s]
W_q	weight of floating ring [N]
X, Y	inertia coordinate system
ρ	fluid density [kg/m^3]
μ	fluid viscosity [Ns/m^2]
Ω	rotor whirl frequency [1/s]
ϖ	rotor angular velocity [1/s]
ε_0	shaft eccentricity ratio, $e_0/\bar{C}$
$\Delta\varepsilon_x$, $\Delta\varepsilon_y$	dimensionless perturbed eccentricities
ΔP	pressure drop of the floating ring seal [MPa] , P_r-P_s

Subscripts

0	zeroth-order solution
α	first-order perturbations in X, Y directions
z, *θ*	axial and circumferential coordinate system

NUMERICAL SOLUTION OF THE FLOATING RING SEAL

A floating ring seal is free to move in X, Y, and θ directions as illustrated in Figure 2**.** However, the seal could be defined as an eccentric annular seal when it is locked up.

The Bulk-Flow Model

The bulk-flow model is a development of the thin-film theory. It was first proposed by Childs [10-11] for the turbulent bulk flow on the annular seal region. The present derivation is based on Moody's friction factor formulas introduced by Nelson and Nguyen [12-14]. The model for the shear stress includes the local effect of Reynolds number and surface roughness.

$$\frac{\partial H}{\partial t}+\frac{1}{R}\frac{\partial(HU_\theta)}{\partial\theta}+\frac{\partial(HU_z)}{\partial Z}=0 \tag{1}$$

$$-\frac{H}{\rho}\frac{\partial P}{\partial Z}=\frac{1}{2}U_z U_s f_s+\frac{1}{2}U_z U_r f_r + H\left(\frac{\partial U_z}{\partial t}+\frac{U_\theta}{R}\frac{\partial U_z}{\partial\theta}+U_z\frac{\partial U_z}{\partial Z}\right) \tag{2}$$

$$-\frac{H}{\rho R}\frac{\partial P}{\partial\theta}=\frac{1}{2}U_\theta U_s f_s+\frac{1}{2}(U_\theta-Rw)U_r f_r + H\left(\frac{\partial U_\theta}{\partial t}+\frac{U_\theta}{R}\frac{\partial U_\theta}{\partial\theta}+U_z\frac{\partial U_\theta}{\partial Z}\right) \tag{3}$$

U_s and U_r are the bulk-flow velocities relative to the wall and are defined as:

$$U_S=\left(U_z^2+U_\theta^2\right)^{1/2} \tag{4}$$

$$U_r=\left[U_z^2+(U_\theta-R\omega)^2\right]^{1/2} \tag{5}$$

The Moody friction factors are defined as:

$$f_S=a_1\left[1+\left(\frac{b_2 e_S}{2H}+\frac{b_3}{R_S}\right)^{1/3}\right] \tag{6}$$

$$f_r=a_1\left[1+\left(\frac{b_2 e_r}{2H}+\frac{b_3}{R_r}\right)^{1/3}\right] \tag{7}$$

where $a_1=1.375\times10^{-3}$, $b_2=2\times10^4$, $b_3=10^6$.

Perturbation Analysis

The dynamic operating regime is traditionally described as a small amplitude motion of the rotor about an equilibrium position. For displacement perturbation, the film thickness h is described in

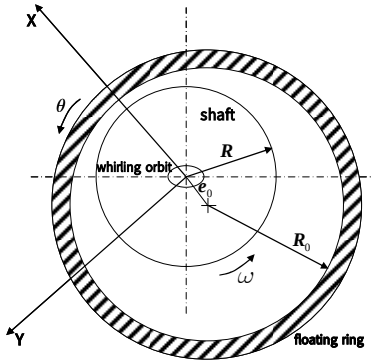

Figure 2. Coordinate of a floating ring seal.

dimensionless form by the real part of the following equation:

$$h=h_0+\exp(j\omega t)(\Delta\varepsilon_X\cos\theta+\Delta\varepsilon_Y\sin\theta) \tag{8}$$

Following the traditional small perturbation method, all variables are decomposed as following equation.

$$\Phi=\Phi_0+\exp(j\omega t)(\Delta\varepsilon_x\Phi_x+\Delta\varepsilon_y\Phi_y) \tag{9}$$

The introduction of this decomposition yields two systems of equations. The zeroth-order part is the original system with the exception of the unsteady terms. Calculation of the zeroth-order equations yields the leakage flowrate, attitude angle and hydrodynamic reactive force. The first-order system consists of the following linear equations and uses the resulting zeroth-order variables as input.

$$j\Omega Th_\alpha+\frac{bL}{R}\frac{\partial h_0}{\partial\theta}u_{\theta\alpha}+\frac{bL}{R}h_0\frac{\partial u_{\theta\alpha}}{\partial\theta}+h_0\frac{\partial u_{z\alpha}}{\partial z}+\gamma_\alpha=0 \tag{10}$$

$$\gamma_{11}u_{z\alpha}+\gamma_{12}u_{\theta\alpha}+b\,L\!\!\not\!/\,R\,u_{\theta 0}h_0\frac{\alpha u_{z\alpha}}{\partial\theta}+h_0u_{z0}\frac{\alpha u_{z\alpha}}{\partial z}=-h_0\frac{\alpha p_\alpha}{\partial z}+\gamma_{1\alpha} \tag{11}$$

$$\gamma_{21}u_{z\alpha}+\gamma_{22}u_{\theta\alpha}+b\,L\!\!\not\!/\,R\,u_{\theta 0}h_0\frac{\alpha u_{\theta\alpha}}{\partial\theta}+h_0u_{z0}\frac{\alpha u_{\theta\alpha}}{\partial z}=-\,h_0\!\!\not\!/\,b\;L\!\!\not\!/\,R\frac{\alpha p_\alpha}{\partial\theta}+\gamma_{2\alpha} \tag{12}$$

where α=X, Y.

The coefficients γ_{11}, γ_{12}, γ_α etc., are functions of zeroth-order input data and friction factors, and are given in detail in the appendix. Forces arising from perturbation are obtained by integrating the first-order pressure field and are expressed via the dynamic coefficients: The dynamic coefficients are evaluated from a least square procedure by using the results obtained for two exciting frequencies (zero and synchronous whirl).

$$-\begin{Bmatrix}F_X^{(1)}\\F_Y^{(1)}\end{Bmatrix}=\begin{bmatrix}K_{XX}&K_{XY}\\K_{YX}&K_{YY}\end{bmatrix}\begin{Bmatrix}\Delta\varepsilon_X\\\Delta\varepsilon_Y\end{Bmatrix}+\begin{bmatrix}C_{XX}&C_{XY}\\C_{YX}&C_{YY}\end{bmatrix}\begin{Bmatrix}\Delta\dot\varepsilon_X\\\Delta\dot\varepsilon_Y\end{Bmatrix}+\begin{bmatrix}M_{XX}&M_{XY}\\M_{YX}&M_{YY}\end{bmatrix}\begin{Bmatrix}\Delta\ddot\varepsilon_X\\\Delta\ddot\varepsilon_Y\end{Bmatrix} \tag{13}$$

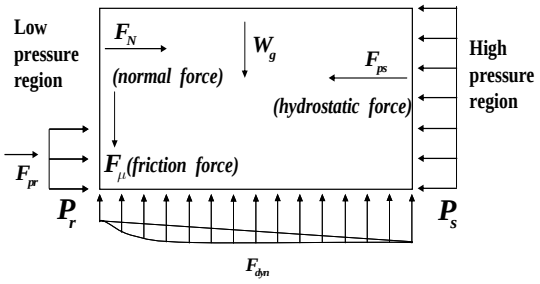

Figure 3. Floating ring's force balance.

Numerical Procedure

A finite difference scheme was used to solve the nonlinear governing equations. A numerical solution for the bulk-flow system of equations and adapted in order to take into account the elliptic character of the pressure field was first proposed in [15] and was further used for analyzing straight seals by San Andres. The procedure is based on the finite difference scheme and the SIMPLE algorithm used for accelerating convergence in the solution of the difference equations. A staggered grid is generated. The velocity components are calculated for the points that lie on the faces of the control volumes. Discrete algebraic forms of the momentum and continuity equations are obtained by integration of the governing differential equations. The key points of the algorithm are a velocity correction approach developed from the momentum equations and a pressure correction approach developed from the continuity equations.

The zeroth-order equations based on the above procedure were calculated at an eccentricity ratio assumed to be close to the actual lock-up eccentricity ratio of the floating ring seal. The lock-up eccentricity ratio depends on the geometric parameters of the floating ring, the surface friction coefficient between the supporting and floating rings, and the operating conditions of the turbo pump. Using a steepest descent method, the zeroth-order procedure is calculated iteratively to find the exact lock-up eccentricity ratio. The system of the first-order bulk-flow equations is solved by using the same modified SIMPLE algorithm.

Floating Ring Seal's Equilibrium Condition

The floating ring will float to the geometric center of the rotor

before the hydrodynamic force is equal to the resultant force. In Figure 3, the force balance between the hydrodynamic and the resultant force determines the lock-up eccentric ratio of the floating ring seal. The force balance equations have been explained by Ha *et al.*

$$F_{\mu}+W_g-F_{dyn}(\varepsilon_0)=0 \tag{14}$$

Using a steepest descent method, the object function is defined as:

$$I(\varepsilon_0)=abs(F_{\mu}+W_g-F_{dyn}(\varepsilon_0)) \tag{15}$$

The goal is to find the right ε_0 to achieve minimum $I(\varepsilon_0)$, with a small perturbation on $I(\varepsilon_0)$, $(\varepsilon_0)new=\varepsilon_0+\Delta\varepsilon_0$.

The slope of the change in $I(\varepsilon_0)$ is found:

$$\frac{dI}{d\varepsilon_0}=\frac{I_{new}-I}{\Delta\varepsilon_0} \tag{16}$$

From this initial value, ε_0 is adjusted by following the slope to decrease the object function:

$$(\varepsilon_0)_{new}=\varepsilon_0+\alpha\frac{d\varepsilon_0}{dI}I(\varepsilon_0) \tag{17}$$

where α is a relaxation coefficient.

$(\varepsilon_0)_{new}$ then will be updated iteratively along the gradient of the function $I(\varepsilon_0)$ until the object function reaches its minimum values. When the process converges, we get the floating ring seal's equilibrium position.

COMPARISONS WITH PREDICTIONS FROM HA *et. al.*(2002) AND EXPERIMENTAL DATA

The theoretical results obtained with the method introduced above are compared with Ha's results and experimental data taken from the reference [9]. These data consist of lock-up eccentricity ratios, attitude angles, leakage flowrates and rotordynamic coefficients. The floating ring seals were fed with water (ρ=997.1 kg/m^3, μ=0.000894 Ns/m^2) at three pressure drops (3.0 MPa, 5.0 MPa and 7.0 MPa) across the seal and at four rotating speeds (6200 rpm, 12400 rpm, 18600 rpm and 24800 rpm). The surface roughness coefficient between the floating ring and the supporting ring is 0.1. The geometric characteristics of the seal are as followings: the radius of the rotor is 26.5 mm; the radius of the

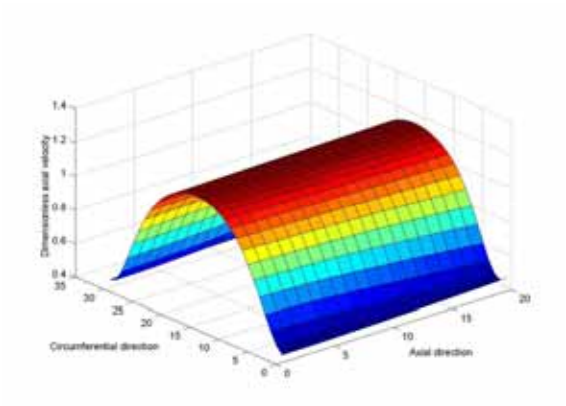

Figure 4. Axial velocity distribution of the floating ring seal (pressure drop ΔP =5.0 MPa, operating speed is 18600 rpm , rotor radius R=26.5 mm, seal length L=8 mm).

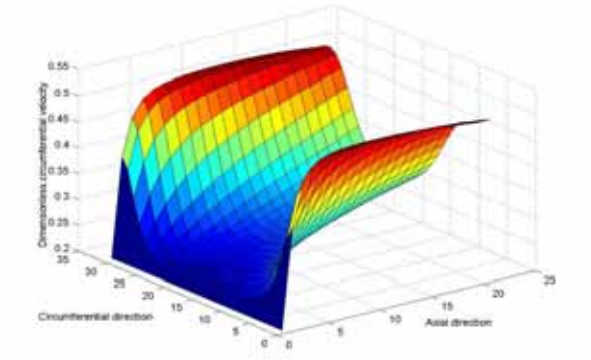

Figure 5. Circumferential velocity distribution of the floating ring seal (pressure drop ΔP =5.0 MPa, operating speed is 18600 rpm , rotor radius R=26.5 mm, seal length L=8 mm).

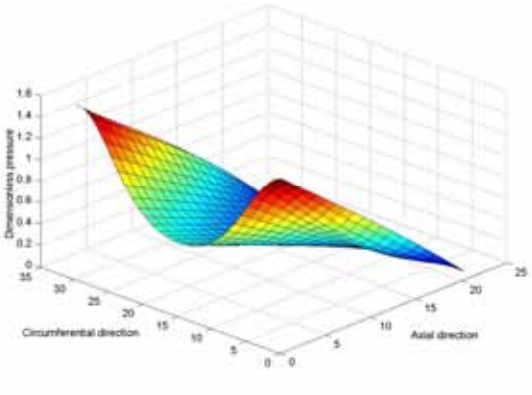

Figure 6. Pressure distribution of the floating ring seal (pressure drop ΔP =5.0 MPa, operating speed is 18600 rpm , rotor radius R=26.5 mm, seal length L=8 mm).

supporting ring is 28 mm; the length of the seal is 8 mm; the height of the seal is 4.5 mm; and the clearance is 0.0875 mm. Considering the seal geometry and the test results, the inlet pressure loss coefficient is 0.7 and the inlet swirl ratio is 0.2 (pressure drop is 5.0 MPa).

These constants express the interaction of the seal flow and are affected by the pressure drop. The agreement between the theoretical and experimental lock-up eccentricity ratio, leakage flowrate and attitude angle was considered as minimal requirements for comparing rotordynamic coefficients.

Figures 4 to 6 show the zeroth-order velocity and pressure field distributions. The number of control volumes in the circumferential direction is 30 and in the axial direction is 20. Figure 4 shows that in the interior of the seal ($\theta=180^0$), where the clearance is highest, the fluid flows more quickly in the axial direction than at the edges ($\theta=0^0$, $\theta=360^0$). Figure 5 shows that at the edges, the fluid flows more quickly in the circumferential direction, because the fluid must keep mass continuity.

Also along the axial direction, the shaft's rotating effect will increase the circumferential velocity. Figure 6 illustrates the hydrostatic stiffening effect of the seal due to the inlet pressure loss effect and the axial pressure gradient, which develops significant direct stiffness.

Figure 7 depicts the influence of the rotating speed and pressure drop on the lock-up eccentricity ratio. Eight working regimes were considered for comparing the present analysis with Ha's predictions, corresponding to the lowest and highest pressure drops across the seal, and to the four working operating speeds. High pressure drops generate large hydrodynamic force and large friction force. However the increase of the friction force is not as big as the hydrodynamic force by the analytic result, so it will move the seal to the geometric center of the rotor. Consequentially the lock-up eccentricity ratio decreases to achieve a force equilibrium, which can easily be seen in the figure. However, in the working conditions with highest pressure drops, present analysis did not closely match the test results, though it was an improvement compared to Ha's results. This is presumed to be because the exit pressure recovery effect can not be ignored in a high pressure drop situation.

Figure 8 depicts the decrease in the leakage flowrate by rotating speed, which increases significantly with the pressure drop. This behavior denotes that the leakage flowrate is mainly affected by the

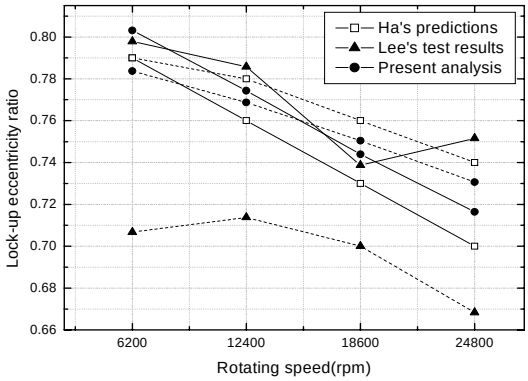

Figure 7. Lock-up eccentricity ratio (solid lines: pressure drop ΔP =3.0 MPa, dashed lines: pressure drop ΔP =7.0 MPa).

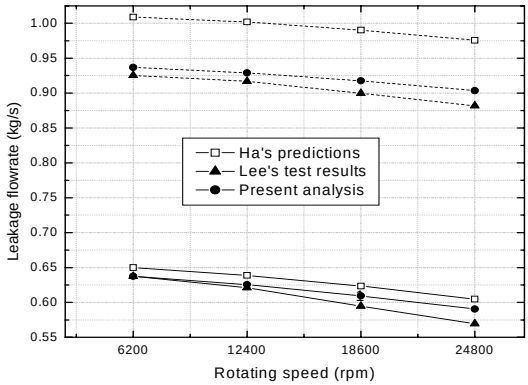

Figure 8. Leakage flow rate (solid lines: pressure drop ΔP =3.0 MPa, dashed lines: pressure drop ΔP =7.0 MPa).

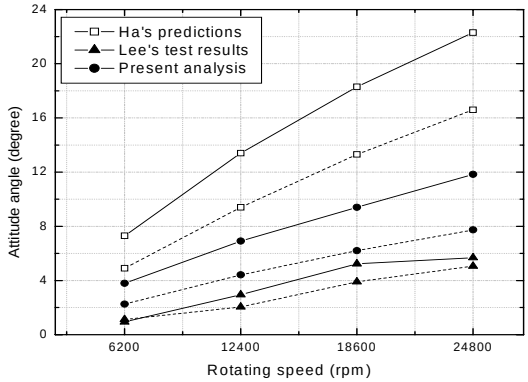

Figure 9. Attitude angle (solid lines: pressure drop ΔP =3.0 MPa, dashed lines: pressure drop ΔP =7.0 MPa).

axial velocity, and the circumferential velocity has a damping effect on the fluid's flow across the seal. Figure 9 depicts the increases in attitude angle by rotating speed and decreases with the pressure drop. Note that results of the analysis are larger than the results of the test. The differences arise as a result of the low pressure drop. Figures 10 and 11 show the influence of the rotating speed on the stiffness coefficients for the middle pressure drop, Δp=5.0 MPa. The direct stiffness coefficients are larger than the cross-coupled stiffness coefficients for the entire operating speed range. This behavior denotes the dominance of hydrostatic stiffening effect on the performance of floating ring seals. The direct stiffness K_{xx} increases as the rotating speed increases. K_{xy} and K_{yy} show less sensitivity to rotating speed. Note that K_{yx} is negative in the present analysis, similar to Ha's results, but did not match the test results well.

And K_{yy} is under predicted in the present model. Figures 12 and 13 show the variations in the predicted damping coefficients by increasing rotating speed. The present analysis compares well with the test results and is a considerable improvement over those obtained by Ha. The direct damping coefficients are larger than the cross-coupled damping coefficients for the entire range of operating speeds. Note that predicted C_{yx} decreases as the rotating speed increases, which shows a contrary trend to the test results. Both models produced relatively under predicted inertia coefficients. However, because the inertia coefficients have little influence on the dynamic performance of floating ring seals when compared to stiffness and damping coefficients and the value is very small, the figure is omitted here.

CONCLUSIONS

A numerical procedure for computing the static and dynamic characteristics of floating ring seals is presented. A finite differential method has been implemented to solve the bulk-flow model in eccentric working conditions. Figures 4-6 show the static velocities and pressure field distributions inside the floating ring seal. The effects of pressure drops and rotating speeds on the performance of the floating ring seal are presented as a test case. The effects of rotating speeds, surface friction coefficients, floating ring heights and floating ring seal lengths on the performance of the floating ring seal were thoroughly explained in Ha's paper, and were not further detailed. Predictions of the lock-up eccentricity ratio, leakage flowrate, attitude angle, and hydrodynamic coefficients compared

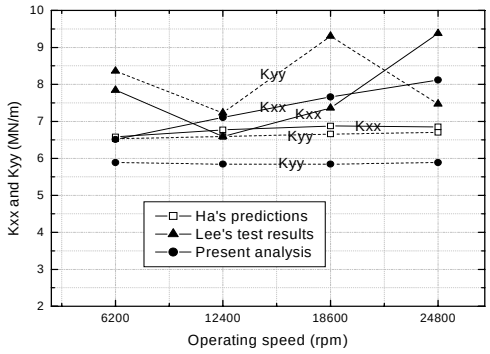

Figure 10. Direct stiffness coefficients versus rotating speed (pressure drop ΔP =5.0 MPa, solid lines: K_{xx}, dashed lines: K_{yy}).

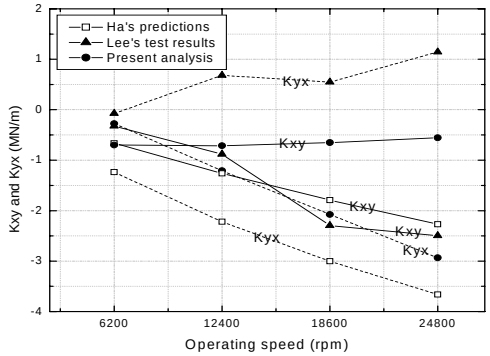

Figure 11. Cross stiffness coefficients versus rotating speed (pressure drop ΔP =5.0 MPa, solid lines: K_{xy}, dashed lines: K_{yx}).

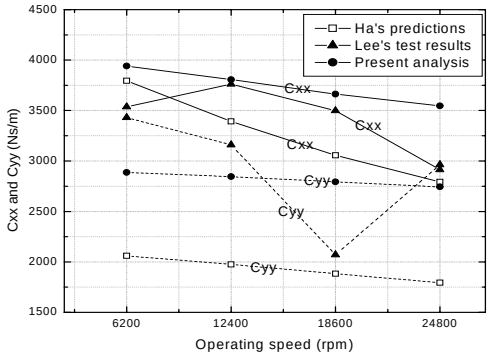

Figure 12. Direct damping coefficients versus rotating speed (pressure drop ΔP =5.0 MPa, solid lines: C_{xx}, dashed lines: C_{yy}).

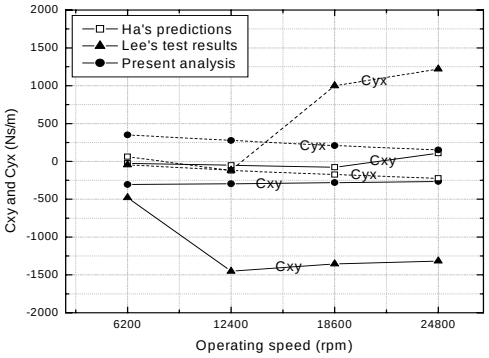

Figure 13. Cross damping coefficients versus rotating speed (pressure drop ΔP =5.0 MPa, solid lines: C_{xy}, dashed lines: C_{yx}).

well with Ha's results and the experimental data taken from the reference[9]. Predictions were better for working conditions with lower pressure drops than for the ones with higher pressure drops. This suggests that the exit pressure recovery effect or the discharge-inertia effect has notable influence over working conditions with high pressure drops. Lock-up eccentricity ratios and leakage flowrates decreased as rotating speeds increased, although the finite differential model more accurately predicts better lock-up eccentricity ratios, less leakage flowrates and attitude angles than the Fast Fourier Transform model. Generally, stiffness and damping coefficients were closer to the test results when compared to Ha's Fast Fourier Transform model, though K_{yx} was negative and C_{yx} decreased as rotating speed increased. Direct inertia coefficients were highly under predicted in both models.

Acknowledgements

This work is supported by grants from the Dual Use Technology Program and the Korea Space Launch Vehicle-I (KSLV-I) Program of the Ministry of Science and Technology, Republic of Korea and a collaborative project between Korea Institute of Science and Technology and Tsinghua University.

REFERENCES

1. Kirk, G., and Miller, H., 1979, "The Influence of High Pressure Oil Seals on Turbo-Rotor Stability," ASLE Trans, Vol. 22, 1, pp. 14-24.
2. Kirk, G., 1986, "Oil Seal Dynamics: Considerations for Analysis of Centrifugal Compressors," Proceedings of 15th Texas A&M Turbomachinery Symposium, Texas A&M University, pp. 10-13.
3. Tae-Woong Ha., Yong-Bok Lee., and Chang-Ho Kim., 2002, "Leakage and Rotordynamic Analysis of a High Pressure Floating Ring Seal in the Turbo Pump Unit of a Liquid Rocket Engine," Tribology International., 35, pp. 153-161.
4. Childs, D., and Kim, C., 1985, "Analysis and Testing for Rotordynamic Coefficients of Turbulent Annular Seals with Different, Directionally-Homogeneous Surface Roughness Treatment for Rotor and Stator Elements," ASME Journal of Tribology, Vol. 107, 3, pp. 296-306.
5. Childs, D., and Dressman, J. B., 1985, "Convergent-Tapered Annular Seals: Analysis and Testing for Rotrodynamic Coefficients," ASME Journal of Tribology, Vol. 107, 3, pp. 307-317.
6. Childs, D., Nolan, S., and Nunez, D., 1988, "Clearance Effects on Leakage and Rotordynamic Coefficients of Smooth, Liquid Annular Seals," Proceedings of the Inst. of Mechanical Engineers, Paper C315/88, pp. 371-377.
7. Luis A. San Andres, 1991, "Analysis of Variable Fluid Properties, Turbulent Annular Seals," Transactions of the ASME, Vol. 113, pp. 694-702.
8. Van Doormaal. J. P., and Raithby. G. D., 1984, "Enhancements of the SIMPLE Method for Predicting Incompressible Fluid Flows," Numerical Heat Transfer, Vol. 7, pp.147-163.
9. Y B Lee., S K Shin., K Ryu., C H Kim., and Gunhee Jang., 2005, "Test Results for Leakage and Rotordynamic Coefficients of Floating Ring Seals in a High Pressure, High Speed Turbopump," Tribology Transactions, Vol. 48, 3, pp. 273-282
10. Childs, D. W., 1983, "Dynamic Analysis of Turbulent Annular Seals Based on Hirs Lubrication Equation," ASME Journal of Lubrication Technology, Vol. 105, pp. 429-436.
11. Childs, D. W., 1983, "Finite Length Solutions for Rotordynamic Coefficients of Turbulent Annular Seals," ASME Journal of Lubrication Technology, Vol. 105, pp. 437-444.
12. Nelson, C., and Nguyen, B., 1987, "Comparison of Hirs'

Equation with Moody's Equation for Determining Rotordynamic Coefficients of Annular Pressure Seals," ASME Journal of Tribology, Vol. 109, pp.144-148.

13. Nelson, C., and Nguyen, B., 1988, "Analysis of Eccentric Annular Seals: Part I-A New Solution Using Fast Fourier Transforms for Determining Hydrodynamic Force," ASME Journal of Tribology, Vol. 110, pp. 355-366.
14. Nelson, C., and Nguyen, B., 1988, "Analysis of Eccentric Annular Seals: Part II-Effects of Eccentricity on Rotordynamic Coefficients," ASME Journal of Tribology, Vol. 110, pp. 361-366.
15. Launder, B. E., and Leschziner, M., 1978, "Flow in Finite-Width, Thrust Bearings Including Inertial Effects," ASME J. Lubr. Technol., 100, pp. 330-338.

APPENDIX. PERTURBATION COEFFICIENTS

$$\gamma_x = -b\,L/R\,u_{\theta 0}h_y + b\,L/R\,\frac{\partial u_{\theta 0}}{\partial \theta}h_x + \frac{\partial u_{z0}}{\partial z}h_x \tag{1}$$

$$\gamma_y = b\,L/R\,u_{\theta 0}h_x + b\,L/R\,\frac{\partial u_{\theta 0}}{\partial \theta}h_y + \frac{\partial u_{z0}}{\partial z}h_y \tag{2}$$

$$\begin{aligned}\gamma_{11} &= -\frac{a_1 a_3 u_{z0}^2}{6B_{s0}^{2/3}h_0 u_{s0}^2}\,L/\bar{C} + \frac{1}{2}u_{s0}f_{s0}\,L/\bar{C} \\ &+ \frac{1}{2}\frac{u_{z0}^2 f_{s0}}{u_{s0}}\,L/\bar{C} - \frac{a_1 a_3 u_{z0}^2}{6B_{r0}^{2/3}h_0 u_{r0}^2}\,L/\bar{C} + \frac{1}{2}u_{r0}f_{r0}\,L/\bar{C} \\ &+ \frac{1}{2}\frac{u_{z0}^2 f_{r0}}{u_{r0}}\,L/\bar{C} + h_0\frac{\partial u_{z0}}{\partial z} + j\Omega T h_0\end{aligned} \tag{3}$$

$$\begin{aligned}\gamma_{12} &= -\frac{a_1 a_3 b^2 u_{z0}u_{\theta 0}}{6B_{s0}^{2/3}h_0 u_{s0}^2}\,L/\bar{C} + \frac{1}{2}\frac{b^2 u_{z0}u_{\theta 0}f_{s0}}{u_{s0}}\,L/\bar{C} \\ &- \frac{a_1 a_3 b^2 u_{z0}\left(u_{\theta 0}-1\right)}{6B_{r0}^{2/3}h_0 u_{r0}^2}\,L/\bar{C} + \frac{1}{2}\frac{b^2 u_{z0}\left(u_{\theta 0}-1\right)f_{r0}}{u_{r0}}\,L/\bar{C} \\ &+ b\,L/R\,h_0\frac{\partial u_{z0}}{\partial \theta}\end{aligned} \tag{4}$$

$$\begin{aligned}\gamma_{1\alpha} &= -\frac{\partial p_0}{\partial z}h_\alpha + \frac{a_1 u_{z0}u_{s0}B_{s0}^{1/3}}{6h_0}h_\alpha\,L/\bar{C} \\ &+ \frac{a_1 u_{z0}u_{r0}B_{r0}^{1/3}}{6h_0}h_\alpha\,L/\bar{C} - b\,L/R\,u_{\theta 0}\frac{\partial u_{z0}}{\partial \theta}h_\alpha \\ &- u_{z0}\frac{\partial u_{z0}}{\partial z}h_\alpha\end{aligned} \tag{5}$$

$$\begin{aligned}\gamma_{21} &= -\frac{a_1 a_3 u_{\theta 0}u_{z0}}{6B_{s0}^{2/3}h_0 u_{s0}^2}\,L/\bar{C} + \frac{1}{2}\frac{u_{\theta 0}u_{z0}f_{s0}}{u_{s0}}\,L/\bar{C} \\ &- \frac{a_1 a_3 u_{\theta 0}u_{z0}\left(u_{\theta 0}-1\right)}{6B_{r0}^{2/3}h_0 u_{r0}^2}\,L/\bar{C} + \frac{1}{2}\frac{u_{z0}\left(u_{\theta 0}-1\right)f_{r0}}{u_{r0}}\,L/\bar{C} \\ &+ h_0\frac{\partial u_{\theta 0}}{\partial z}\end{aligned} \tag{6}$$

$$\begin{aligned}\gamma_{22} &= -\frac{a_1 a_3 b^2 u_{\theta 0}^2}{6B_{s0}^{2/3}h_0 u_{s0}^2}\,L/\bar{C} + \frac{1}{2}u_{s0}f_{s0}\,L/\bar{C} + \frac{1}{2}\frac{b^2 u_{\theta 0}^2 f_{s0}}{u_{s0}}\,L/\bar{C} \\ &- \frac{a_1 a_3 b^2\left(u_{\theta 0}-1\right)^2}{6B_{r0}^{2/3}h_0 u_{r0}^2}\,L/\bar{C} + \frac{1}{2}u_{r0}f_{r0}\,L/\bar{C} \\ &+ \frac{1}{2}\frac{b^2\left(u_{\theta 0}-1\right)^2 f_{r0}}{u_{r0}}\,L/\bar{C} + b\,L/R\,h_0\frac{\partial u_{\theta 0}}{\partial \theta} + j\Omega T h_0\end{aligned} \tag{7}$$

$$\begin{aligned}\gamma_{2\alpha} &= -L/bR\,\frac{\partial p_0}{\partial \theta}h_\alpha + \frac{a_1 u_{\theta 0}u_{s0}B_{s0}^{1/3}}{6h_0}h_\alpha\,L/\bar{C} \\ &+ \frac{a_1\left(u_{\theta 0}-1\right)u_{r0}B_{r0}^{1/3}}{6h_0}h_\alpha\,L/\bar{C} - b\,L/R\,u_{\theta 0}\frac{\partial u_{\theta 0}}{\partial \theta}h_\alpha \\ &- u_{z0}\frac{\partial u_{\theta 0}}{\partial z}h_\alpha\end{aligned} \tag{8}$$

where: α =x, y; $h_\alpha = \left\{h_x = \cos\theta;\quad h_y = \sin\theta\right\}$

$$B_{s0} = \frac{a_{2s}}{h_0} + \frac{a_3}{h_0 u_{s0}};\quad B_{r0} = \frac{a_{2r}}{h_0} + \frac{a_3}{h_0 u_{r0}}$$

and,

$$a_{2s} = \frac{b_2 e_s}{2\bar{C}};\qquad a_{2r} = \frac{b_2 e_r}{2\bar{C}}$$